Draft version December 10, 2019
Preprint typeset using LaTeX style emulateapj v. 12/16/11

FULL TRANSPORT GENERAL RELATIVISTIC RADIATION MAGNETOHYDRODYNAMICS FOR NUCLEOSYNTHESIS IN COLLAPSARS

Jonah M. Miller
Computational Physics and Methods, Los Alamos National Laboratory, Los Alamos, NM, USA
Center for Theoretical Astrophysics, Los Alamos National Laboratory, Los Alamos, NM, USA and
Center for Nonlinear Studies, Los Alamos National Laboratory, Los Alamos, NM, USA

Trevor M. Sprouse
Los Alamos Center for Space and Earth Science Student Fellow
Department of Physics, University of Notre Dame, Notre Dame, IN, USA and
Theoretical Divison, Los Alamos National Laboratory, Los Alamos, NM 87545, USA

Christopher L. Fryer
Computational Physics and Methods, Los Alamos National Laboratory, Los Alamos, NM 87545, USA and
Center for Theoretical Astrophysics, Los Alamos National Laboratory, Los Alamos, NM 87545, USA

Benjamin R. Ryan
Computational Physics and Methods, Los Alamos National Laboratory, Los Alamos, NM, USA and
Center for Theoretical Astrophysics, Los Alamos National Laboratory, Los Alamos, NM, USA

Joshua C. Dolence
Computational Physics and Methods, Los Alamos National Laboratory, Los Alamos, NM, USA and
Center for Theoretical Astrophysics, Los Alamos National Laboratory, Los Alamos, NM, USA

Matthew R. Mumpower
Theoretical Divison, Los Alamos National Laboratory, Los Alamos, NM 87545, USA and
Center for Theoretical Astrophysics, Los Alamos National Laboratory, Los Alamos, NM 87545, USA

Rebecca Surman
Department of Physics, University of Notre Dame, Notre Dame, IN, USA
Draft version December 10, 2019

ABSTRACT

We model a compact black hole-accretion disk system in the collapsar scenario with full transport, frequency dependent, general relativistic radiation magnetohydrodynamics. We examine whether or not winds from a collapsar disk can undergo rapid neutron capture (r-process) nucleosynthesis and significantly contribute to solar r-process abundances. We find the inclusion of accurate transport has significant effects on outflows, raising the electron fraction above $Y_e \sim 0.3$ and preventing third peak r-process material from being synthesized. We compare our model to semi-analytic expectations and argue that accurate neutrino transport and realistic initial and boundary conditions are required to capture the dynamics and nucleosynthetic outcome of a collapsar.

1. INTRODUCTION

When a massive rapidly rotating star collapses, it may fail to explode and cut off accretion before the proto-neutron star collapses and forms a black hole. In this scenario, stellar material eventually circularizes and accretes onto the central black hole. Woosley (1993) coined this a "failed" supernova, with "failed" in quotes, since an accretion-driven jet may indeed cause an explosion. MacFadyen and Woosley (1999) coined this the collapsar scenario, and this system a collapsar. These events are commonly invoked as the sources of long gamma ray bursts (GRBs), and observational evidence is consistent with this hypothesis (Woosley and Bloom 2006; Ghirlanda *et al.* 2009; Hjorth and Bloom 2012).

The dynamics of stellar collapse and the formation of a GRB engine has thus been studied extensively, see Woosley (1993); MacFadyen and Woosley (1999); MacFadyen *et al.* (2001); Proga *et al.* (2003); Heger *et al.* (2003); Mizuno *et al.* (2004); Fujimoto *et al.* (2006); Nagataki *et al.* (2007); Rockefeller *et al.* (2006); Uzdensky and MacFadyen (2007); Morsony *et al.* (2007); Bucciantini *et al.* (2008); Lazzati *et al.* (2008); Kumar *et al.* (2008); Nagakura *et al.* (2011); Taylor *et al.* (2011); Ott *et al.* (2011); Lindner *et al.* (2012); López-Cámara *et al.* (2013); Batta and Lee (2014) and references therein. Recently, attention has been devoted to the related case where a rapidly rotating star collapses to a protoneutron star and black hole formation is either delayed or does

jonahm@lanl.gov

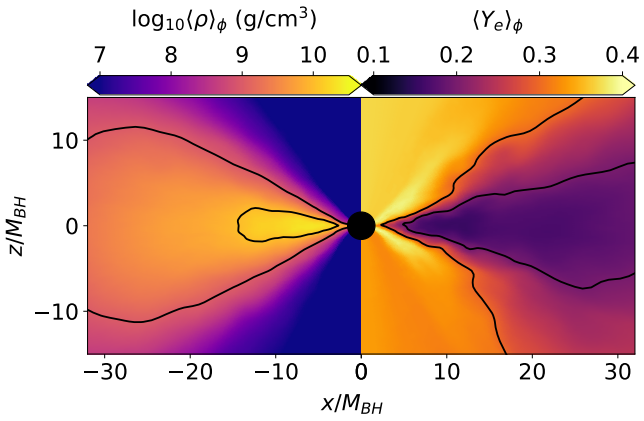

FIG. 1.— Density ρ (left) and electron fraction Y_e (right) at $t = 5 \times 10^3 GM_{BH}/c^3$, or ≈ 74 ms. Contours are for $\rho = 10^9, 10^{10}$ g/cm^3 and $Y_e = 0.2, 0.3$ respectively. Both quantities are averaged over azimuthal angle ϕ.

not happen at all (Thompson *et al.* 2004; Metzger *et al.* 2008; Winteler *et al.* 2012; Mösta *et al.* 2014, 2018; Halevi and Mösta 2018).

MacFadyen and Woosley (1999) realized that the dynamics of collapsar disks are similar to other neutron-rich compact accretion flows such as those formed by a binary neutron star merger. This implies that collapsar disks may be a proposed site of rapid neutron capture or r-process nucleosynthesis, the mechanism by which the heaviest elements in our universe are formed (Blinnikov *et al.* 1984; Lattimer and Schramm 1976; Lattimer *et al.* 1977). Nucleosynthesis in rapidly rotating core collapse—with and without black hole formation—has been explored by several groups (Popham *et al.* 1999; Di Matteo *et al.* 2002; Surman and McLaughlin 2004; McLaughlin and Surman 2005; Surman *et al.* 2006; Thompson *et al.* 2004; Rockefeller *et al.* 2008; Metzger *et al.* 2008; Winteler *et al.* 2012; Mösta *et al.* 2014, 2018; Halevi and Mösta 2018).

For r-process elements to be synthesized, the central engine must produce outflows with low electron fraction Y_e. A robust r-process typically requires $Y_e \lesssim 0.25$. Early semi-analytic work found that collapsar outflows are insufficiently neutron-rich (Popham *et al.* 1999; Di Matteo *et al.* 2002; Surman and McLaughlin 2004; McLaughlin and Surman 2005; Surman *et al.* 2006). In the magnetar case, where no black hole formation occurs, three-dimensional simulations show it is difficult to eject a sufficient amount of low Y_e material (Mösta *et al.* 2014, 2018; Halevi and Mösta 2018).

One proposed mechanism for producing massive, neutron-rich outflows is that material may be entrained in a low-density relativistic jet (Fujimoto *et al.* 2007; Ono *et al.* 2012; Nakamura *et al.* 2015; Soker and Gilkis 2017; Hayakawa and Maeda 2018). One promising aspect of this approach is that material entrained in the jet may have high entropy, which means that it may undergo rapid neutron capture even with higher Y_e. Most of these works assume axisymmetry, which means they do not properly account for the non-axisymmetric kink instability (Mösta *et al.* 2014) and suffer from the anti-dynamo theorem (Cowling 1933; Cowling 1957). Another issue is that if a jet is loaded with too much material, it cannot reach large Lorentz factors, meaning there is a tension between producing a robust jet and producing a sufficient amount of r-process material. It remains to be seen whether this mechanism holds up for realistic three-dimensional models and whether or not it can provide a meaningful contribution to abundances of r-process elements in the universe.

Recently Siegel *et al.* (2019) argued that collapsar fallback and subsequent accretion onto the central black hole can be approximately modeled by a magnetohydrodynamically driven accretion disk. They performed a suite of three-dimensional magnetohydrodynamic simulations, each corresponding to a different accretion rate, and thus a different phase of the core-collapse fallback. They find that the outflow from their simulation with the highest accretion rate is neutron-rich and they use this result to argue that collapsars are a primary source of r-process elements in the universe. In addition to the nucleosynthetic implications, Siegel *et al.* (2019) make an observable prediction about long GRBs. Assuming a long GRB is driven by a collapsar, the radioactive decay of r-process elements from the outflow implies an infra-red excess in the afterglow of such an event.

Siegel *et al.* (2019) modeled neutrino radiation with a leakage scheme (Liebendörfer 2005; O'Connor and Ott 2010). However, neutrino transport can have significant effects on the electron fraction and nucleosynthesis in compact accretion flows (Miller *et al.* 2019a). We therefore wish to see how improved transport effects the collapsar scenario. We model the highest accretion rate and thus densest, highest temperature, lowest electron fraction and most nucleosynthetically optimistic disk from Siegel *et al.* (2019) with full frequency dependent general relativistic neutrino radiation magnetohydrodynamics. We then perform r-process nucleosynthesis calculations on the resulting outflow in post-processing.

We find that neutrino transport has significant effects on the disk outflow. In particular, although rapid neutron capture occurs, Y_e is not low enough in the outflow to produce third-peak r-process material. We also use our model to explore the hypothesis that a compact accretion disk is a sufficiently descriptive surrogate for a full collapsar. Although we are unable to make strong claims on the validity of using a single disk as a proxy for a collapsar, we argue that models with better initial and boundary conditions will continue to lack 3rd-peak r-process elements. However, further work is required to more deeply understand the system as a whole.

In section 2, we describe the physical system we simulate. In section 3, we describe our numerical method and discuss resolution requirements. In section 4, we present results from our simulation, including steady-state disk properties, outflow statistics, and nucleosynthetic yield. In section 5, we examine systematic effects in our simulation. We discuss the importance of full neutrino transport and neutrino absorption in achieving our steady-state disk and outflow properties and we comment on the influence of the initial and boundary conditions and discuss the prospect of outflow material escaping the star. Finally, in section 6, we summarize our results and discuss some implications of our work.

2. THE MODEL

We solve the equations of general relativistic ideal magnetohydrodynamics (MHD)

$$\partial_t \left(\sqrt{-g}\rho_0 u^t\right) + \partial_i \left(\sqrt{-g}\rho_0 u^i\right) = 0 \tag{1}$$

$$\partial_t \left[\sqrt{-g}\left(T^t_{\ \nu} + \rho_0 u^t \delta^t_\nu\right)\right] + \partial_i \left[\sqrt{-g}\left(T^i_{\ \nu} + \rho_0 u^i \delta^t_\nu\right)\right] = \sqrt{-g}\left(T^\kappa_{\ \lambda}\Gamma^\lambda_{\nu\kappa} + G_\nu\right) \ \forall \nu = 0, 1, \ldots, 3 \tag{2}$$

$$\partial_t \left(\sqrt{-g}B^i\right) + \partial_j \left[\sqrt{-g}\left(b^j u^i - b^i u^j\right)\right] = 0 \tag{3}$$

$$\partial_t \left(\sqrt{-g}\rho_0 Y_e u^t\right) + \partial_i \left(\sqrt{-g}\rho_0 Y_e u^i\right) = \sqrt{-g} G_{\rm ye} \tag{4}$$

where the energy-momentum tensor $T^\mu_{\ \nu}$ is assumed to be

$$T^\mu_{\ \nu} = \left(\rho_0 + u + P + b^2\right) u^\mu u_\nu + \left(P + \frac{1}{2}b^2\right)\delta^\mu_\nu - b^\mu b_\nu \tag{5}$$

for metric $g_{\mu\nu}$, rest energy ρ_0 fluid four-velocity u^μ, internal energy density u, pressure P, and Christoffel connection $\Gamma^\alpha_{\beta\gamma}$. (Here and in the remainder of the text, unless otherwise specified, we set $G = c = 1$.)

Equation (1) represents conservation of baryon number. Equation (2) represents conservation of energy-momentum, subject to the radiation four-force G_ν. Equation (3) describes the evolution of magnetic fields, where

$$B^i =^* F^{it} \tag{6}$$

comprise the magnetic field components of the Maxwell tensor $F_{\mu\nu}$ and b^μ is the magnetic field four-vector

$$^*F^{\mu\nu} = b^\mu u^\nu - b^\nu u^\mu. \tag{7}$$

Equation (4) describes the conservation of lepton number. G_{ye} is a source term describing the rate at which lepton density is transferred between the fluid and the radiation field.

We close our system with the SFHo equation of state, described in Steiner *et al.* (2013) and tabulated in O'Connor and Ott (2010), which relates the pressure P and specific internal energy ε to the density ρ, temperature T, and electron fraction Y_e:

$$P = P(\rho, T, Y_e) \tag{8}$$

$$\varepsilon = \varepsilon(\rho, T, Y_e). \tag{9}$$

We evolve ρ and Y_e but not T or P. So at a given time, we find T by inverting equation (9) before plugging it into equation (8) to find P.

We approximate our neutrinos as massless such that they obey the standard radiative transfer equation

$$\frac{D}{d\lambda}\left(\frac{h^3 I_{\epsilon,f}}{\epsilon^3}\right) = \left(\frac{h^2\eta_{\epsilon,f}}{\epsilon^2}\right) - \left(\frac{\epsilon\chi_{\epsilon,f}}{h}\right)\left(\frac{h^3 I_{\epsilon,f}}{\epsilon^3}\right), \tag{10}$$

where $D/d\lambda$ is the derivative along a neutrino trajectory in phase space, $I_{\epsilon,f}$ is the intensity of the neutrino field of flavor $f \in \{\nu_e, \bar{\nu}_e, \nu_x\}$,

$$\chi_{\epsilon,f} = \alpha_{\epsilon,f} + \sigma^a_{\epsilon,f} \tag{11}$$

is the extinction coefficient that combines absorption coefficient $\alpha_{\epsilon,f}$ and scattering extinction $\sigma^a_{\epsilon,f}$ for scattering interaction a and

$$\eta_{\epsilon,f} = j_{\epsilon,f} + \eta^s_{\epsilon,f}(I_{\epsilon,f}) \tag{12}$$

is the emissivity combining fluid emissivity $j_{\epsilon,f}$ and emission due to scattering from $\eta^s_{\epsilon,f}$. Here h is Planck's constant, ϵ is the energy of a neutrino with wavevector k^μ as measured by an observer traveling along a timelike Killing vector η^μ.

Neutrinos can interact with matter via emission, absorption, or scattering. The latter does not change electron fraction Y_e, while the former two do. For emission and absorption, we use the charged and neutral current interactions as tabulated in Skinner *et al.* (2019) and summarized in Burrows *et al.* (2006). Our scattering is implemented as described in Miller *et al.* (2019b).

3. METHODS

We simulate a disk of accretion rate $\dot{M} \approx 10^{-1} M_\odot/s$ in a stationary Kerr black hole spacetime (Kerr 1963) for a black hole of mass $M_{BH} = 3M_\odot$ and dimensionless spin $a = 0.8$, corresponding to the most nucleosynthetically optimistic (and highest $\dot{M}$) case presented in Siegel *et al.* (2019). To form the accretion disk, we begin with a torus in hydrostatic equilibrium (Fishbone and Moncrief 1976) of constant specific angular momentum, constant entropy of $s = 8k_b$/baryon, constant electron fraction $Y_e = 0.5$, and total mass of $M_d = 0.02M_\odot$. These conditions imply our torus has an inner radius of 5.5 GM_{BH}/c^2 and a radius of peak pressure of 12.525 GM_{BH}/c^2. Our torus starts with a single poloidal magnetic field loop with a minimum ratio of gas to magnetic pressure β of 100. As the system evolves, the magneto-rotational instability (MRI, Balbus and Hawley 1991) self-consistently drives the disk to a turbulent state, which provides the turbulent viscosity necessary for the disk to accrete (Shakura and Sunyaev 1973).

We use our code `νbhlight` (Miller *et al.* 2019b), based on `bhlight` (Ryan *et al.* 2015), which uses operator splitting to couple GRMHD via finite volume methods with constrained transport (Gammie *et al.* 2003) to neutrino transport via Monte Carlo methods (Dolence *et al.* 2009). We use a radially logarithmic, quasi-spherical grid in horizon penetrating coordinates, as first presented in Gammie *et al.* (2003) with $N_r \times N_\theta \times N_\phi = 192 \times 168 \times 66$ grid points with approximately 3×10^7 Monte Carlo pack-

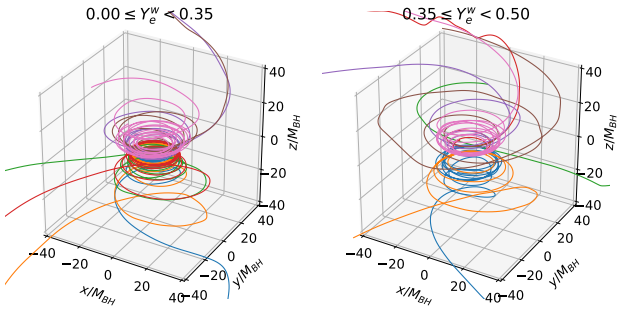

FIG. 2.— Paths of a selection of tracer particles in 3d. We split the tracers into those with $Y_e < 0.35$ (left) and those with $Y_e \geq 0.35$ (right). Broadly, tracers with lower electron fraction spend more time near the polar axis, while tracers with higher electron fraction spend less time. Colors highlight different traces to guide the eye.

ets. Although our code is Eulerian, we track Lagrangian fluid packets with approximately 1.5×10^6 "tracer particles," of which approximately 5×10^5 become gravitationally unbound. Following Bovard and Rezzolla (2017), our tracer particles are initialized within the disk so that they uniformly sample disk material by volume. For more information on our code implementation and verification, see Miller *et al.* (2019b). For a first application of `νbhlight` in the context of neutron star mergers, see Miller *et al.* (2019a).

We run our simulation for approximately $10^4 GM_{BH}/c^3$, or 148 ms, which allows us to observe the disk in a quasistationary turbulent state. In the collapsar paradigm, the disk is fed by circularized fallback from the progenitor star as it undergoes gravitational collapse. The initial phase of our simulation, where we relax an equilibrium torus, comprises an unphysical transient, and we wish to ignore material driven off the disk in this transient phase. We therefore neglect outflow which reaches a surface of $r = 250 GM_{BH}/c^2$ within the first half of the simulation, $t < 5 \times 10^3 GM_{BH}/c^3$. Note that this corresponds to material ejected from the disk at much earlier times. We experimented with the amount of time we neglect and found that it does not significantly change the results presented below.

An accurate magnetohydrodynamic model of turbulent viscosity requires capturing the MRI (Balbus and Hawley 1991). Following Sano *et al.* (2004), we define a quality factor

$$Q^{(\theta)}_{\rm mri} = \frac{2\pi b^{(\theta)}}{\Delta x^{(\theta)} \sqrt{w + b^2} \Omega}, \tag{13}$$

for the MRI to be the number of grid points per minimum unstable MRI wavelength inside the disk. Here $b^{(\theta)}$ is the θ-component of the magnetic field four-vector, $\Delta x^{(\theta)}$ is grid spacing in the θ direction, w is the enthalpy of the fluid, Ω is the angular velocity of the flow, and $b^2 = b^\mu b_\mu$ is total magnetic field strength. To resolve the MRI, one needs at least ten grid points per smallest unstable MRI wavelength (Hawley *et al.* 2013). Our measurements of our disk satisfy this requirement, with $Q^{(\theta)}_{\rm mri} \geq 10$ within the disk for all times.

Our simulation is not only magnetohydrodynamic, but *radiation* magnetohydrodynamic. Therefore, it is important also to ensure we are using a sufficient number of Monte Carlo packets to capture the relevant interactions between the gas and radiation field. Following Miller *et al.* (2019a), we define the Monte Carlo quality factor

$$Q_{\rm rad} = \min_{r,\theta\phi} \left(\frac{\partial N}{\partial t} \frac{u}{J} \right), \tag{14}$$

minimized over the simulation domain. N is the number of emitted Monte Carlo packets, u is gas internal energy density by volume, and J is the total frequency and angle integrated neutrino emissivity. $Q_{\rm rad}$ roughly encodes how well resolved the radiation field is, with $Q_{\rm rad} = 10$ a marginal value. In our simulation, we find $Q_{\rm rad} \gtrsim 100$ for all time.

4. RESULTS

4.1. *Steady-State Structure*

Figure 1 shows the density ρ and electron fraction Y_e in the disk after the transient cutoff of $5 \times 10^3 GM_{BH}/c^3$, which is about 74 ms. The densities closest to the black hole are as large as 10^{10} g/cm^3. In the mid-plane, the disk attains low electron fraction, with $Y_e \sim 0.15$, similar to that in the neutron star merger disk case (Miller *et al.* 2019a). However, at higher latitudes, the electron fraction in the disk is higher.

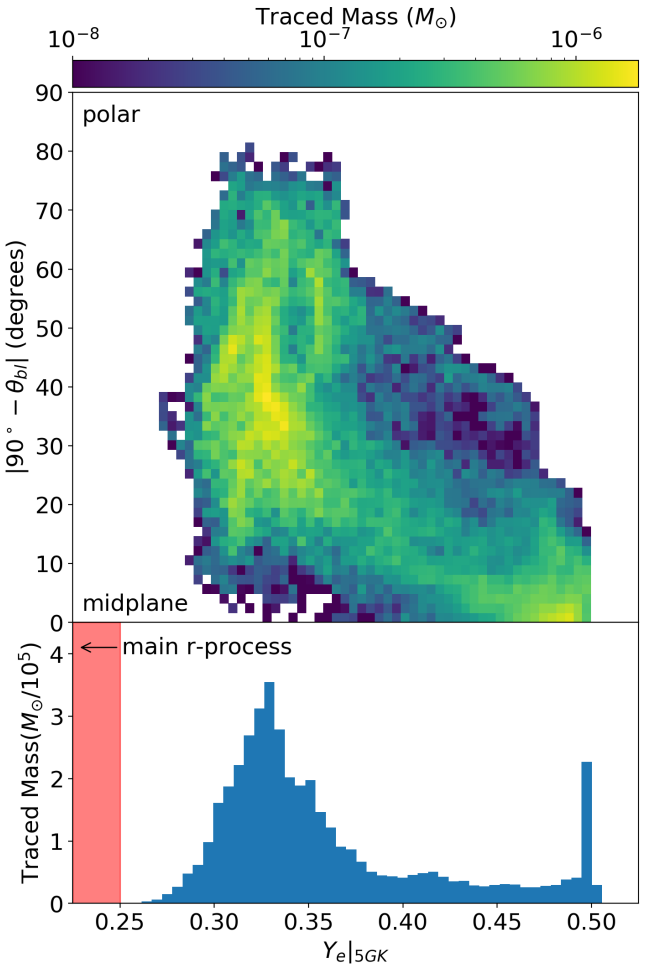

FIG. 3.— Electron fraction Y_e in outflow (top) vs angle and (bottom) binned by mass. The electron fraction is universally large, higher than $Y_e > 0.25$. Y_e is lower for more polar outflow. The spike in $Y_e \approx 0.5$ is from viscous spreading at the back of the disk, which never drops from its initial Y_e to low electron fraction.

4.2. *Outflow*

Figure 2 shows the paths of a selection of gravitationally unbound Lagrangian tracer particles.[1] We split the tracers into those with $Y_e < 0.35$ and those with $Y_e \geq 0.35$. Qualitatively, we find that tracers with lower electron fraction tend to spend more time close to the polar axis. About 1 in 100 tracers have near-vertical trajectories, implying they may be entrained in the jet or that they are interacting with the funnel wall. The prospect of nucleosynthetic material entrained in the jet has been explored in a number of works and is potentially consistent with our results. See Fujimoto *et al.* (2007); Ono *et al.* (2012); Nakamura *et al.* (2015); Soker and Gilkis

[1] Here we define "gravitationally unbound" as reaching an extraction radius of 250 GM_{BH}/c^2 with a positive Bernoulli parameter. More distant choices of extraction radius do not change the results presented here.

(2017); Hayakawa and Maeda (2018) for some examples.

The electron fraction in the outflow is bounded from below by $Y_e \gtrsim 0.25$. The polar outflow has lower electron fraction than the mid-plane outflow, as shown in figure 3. This is in contrast to the neutron star merger case, where the polar outflow had *higher* electron fraction than the mid-plane (Miller *et al.* 2019a). This may or may be related to the different initial conditions—in Miller *et al.* (2019a), the initial torus had $Y_e = 0.1$.

As the disk accretes, magnetically-driven turbulence transports mass in the mid-plane radially inward and angular momentum radially outward. Some material must carry this angular momentum to infinity. The outflow driven by momentum conservation and turbulent viscosity is sometimes referred to as the viscous spreading of the disk. In the neutron star merger case, this viscous spreading is physically meaningful; the disk is not fed, but rather develops from material close to the black hole left over from the merger event. In contrast, in the jet-driven supernova case, the disk is fed by fallback material from the stellar envelope. For completeness, we record this material and count it in our analysis. However, it is not clear that mid-planar outflow will escape the star or that it is physically meaningful.

Although the electron fraction is above $Y_e \sim 0.25$, which is the approximate threshold for robust r-process nucleosynthesis, entropy can play a role in the nucleosynthetic yields as well. In particular, high entropy material may undergo robust r-process even in a less neutron-rich environment. For example, material with entropy of $s = 100 k_b$/baryon and $Y_e = 0.35$ may undergo a robust r-process. High-velocity, shocked material entrained in the jet might become high entropy. Magnetic reconnection in the jet may also drive up entropy. Therefore, we investigate the velocity and entropy of the outflow.

Figure 4 plots the entropy and radial velocity $v_r = \partial r/\partial \tau$ (for proper time τ) of gravitationally unbound material, integrated over simulation time. The angle and radial velocity are measured at an extraction radius of $250 M_{BH}$ or about 1000 km. The entropy is measured when the material drops below a temperature of $5GK$. We find that most material has low entropy, around 17 k_b/baryon, and a velocity of about $0.05c$. Both distributions have short tails, with entropies as large as 65 k_b/baryon and velocities as large as $0.2c$. Note that this is qualitatively different from the neutron star merger case, where both disk wind and dynamical ejecta can move at a significant fraction of the speed of light (Miller *et al.* 2019a). Understanding this difference will be the focus of future work.

Figure 5 compares entropy and velocity with electron fraction in the gravitationally unbound material. Higher entropy material, correlates with lower Y_e while velocity seems roughly uncorrelated.

4.3. *Nucleosynthesis*

For each of the gravitationally unbound tracer particles of Sec. 4.2, we perform nucleosynthesis calculations using the nuclear reaction network Portable Routines for Integrated nucleoSynthesis Modeling (PRISM) (Mumpower *et al.* 2017; Côté *et al.* 2018; Zhu *et al.* 2018; Sprouse *et al.* 2019). For charged particle reaction rates, we implement the Reaclib Database (Cyburt *et al.* 2010). Neutron capture rates are calculated using the Los Alamos National Laboratory (LANL) statistical Hauser-Feshbach code of Kawano *et al.* (2016), assuming nuclear masses of FRDM2012 (Möller *et al.* 2012). Beta-decay properties are similarly calculated using the LANL QRPA+HF framework (Mumpower *et al.* 2016; Mumpower *et al.* 2018; Möller *et al.* 2019). Finally, we supplement these datasets with the nuclear decay properties of the Nubase 2016 evaluation (Audi *et al.* 2017) and AME2016 (Wang *et al.* 2017) where appropriate.

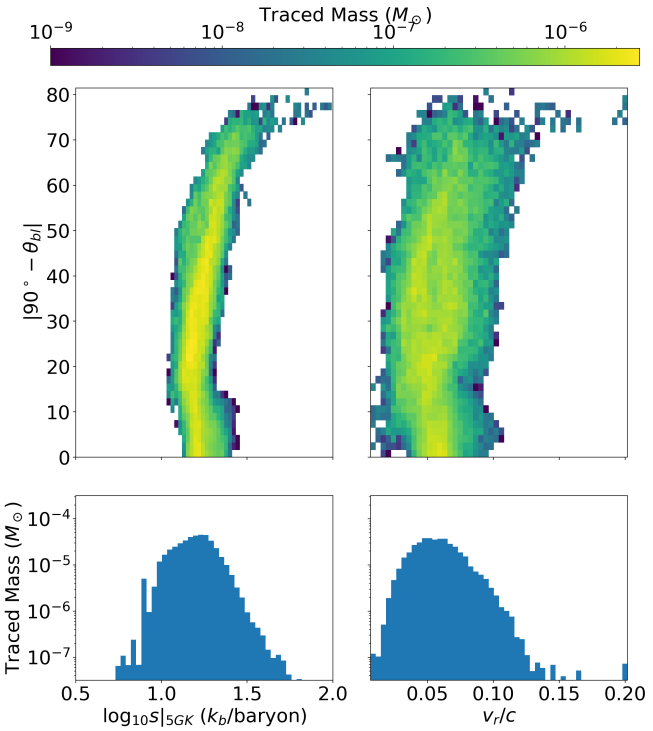

FIG. 4.— Histograms of entropy s (left) and velocity (right) of gravitationally unbound material. The top row compares these quantities to distance from the mid-plane $|90^\circ - \theta_{bl}|$. The bottom simply bins by mass. Most of the material is slow moving and low entropy. However, there is a short tail to the distribution, with entropies as large as 100 k_b/baryon and velocities as large as $0.2c$. This tail is not statistically well-resolved by the number of tracer particles we use.

Figure 6 shows the mass-weighted nucleosynthetic yields at 1 Gyr. As expected given the electron fraction distribution, we find the outflow produces first- and (marginally) second-peak elements but no third-peak elements. Indeed, almost no elements with $A > 130$ are produced. Nucleosynthetic yields vary greatly tracer across tracer particles, however the overall average abundances and the lack of heavy nuclei are robust.

5. SYSTEMATICS

Following Siegel *et al.* (2019), our model assumes that a phase of fallback and subsequent accretion in a collapsar can be mapped to an accretion disk that has relaxed from a compact torus with $Y_e = 0.5$ in hydrostatic equilibrium (Fishbone and Moncrief 1976). [2] (See section 3 for more details.) Here we examine this assumption.

5.1. *How is Material Deleptonized?*

[2] Note that this torus is in *hydrostatic* equilibrium. It is *not* in equilibrium with neutrino radiation field.

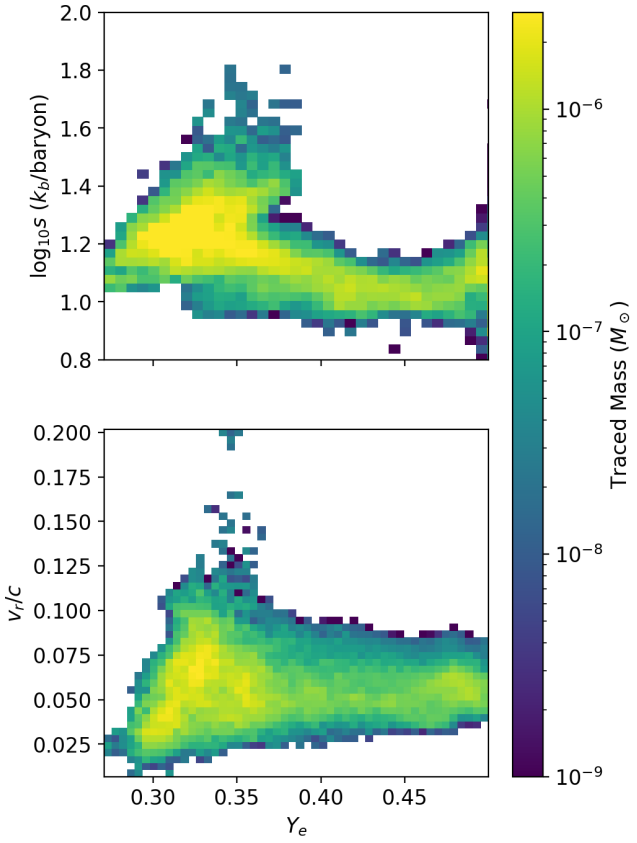

FIG. 5.— Histograms of entropy s (top) and velocity (bottom) vs. electron fraction Y_e for gravitationally unbound material.

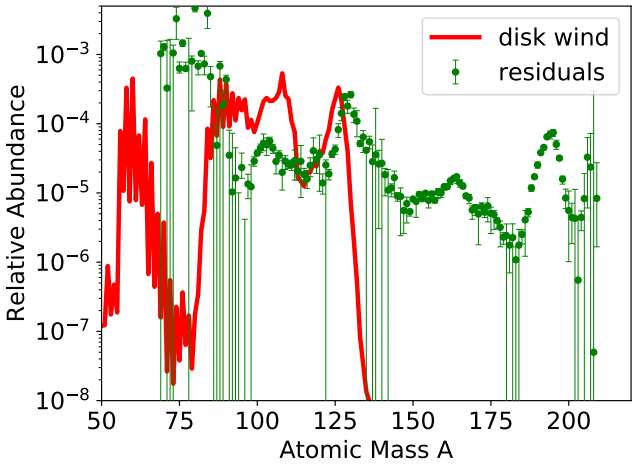

FIG. 6.— Mass-weighted abundances of r-process elements produced in outflow as a function of isotope mass A (red line). Green dots show r-process residuals measured from the solar system in Arnould *et al.* (2007). The outflow produces first and second peak r-process elements, but no third-peak. Almost no elements with $A > 130$ are produced.

Material in our simulation deleptonizes close to the black hole as the initial torus disrupts. In a real collapsar, material deleptonizes as it falls back onto the black hole, potentially from far away. To better understand the effects of the compact torus, we briefly investigate models that do make a more direct fallback assumption.

We examine the model of Popham *et al.* (1999) and

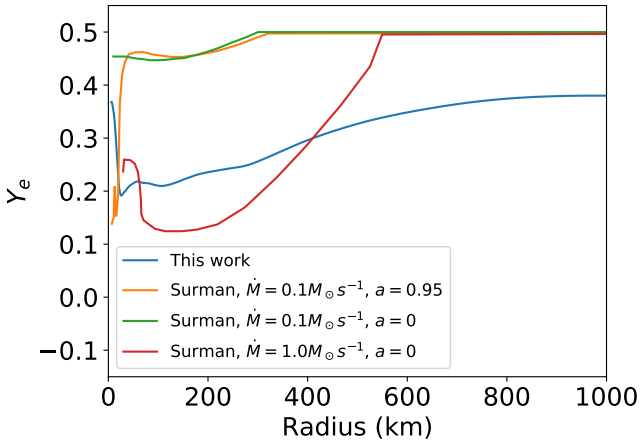

FIG. 7.— Electron fraction as a function of radius for several semi-analytic models, reproduced from (Surman and McLaughlin 2004). For comparison, we include the spherically averaged electron fraction computed in this work.

Di Matteo *et al.* (2002), which analytically incorporates several important neutrino emission and absorption processes and a 5-piece equation of state. These models assume a self-similar thin disk solution beginning at roughly 100km, which forms the outer boundary condition of a steady-state α model (Shakura and Sunyaev 1973). Although this model neglects much of the physics included in our simulation, the important difference in boundary conditions makes it worth discussing.

Neutrino emission and absorption rates can be estimated from the temperature and density in the disk. Surman and McLaughlin (2004) calculated the electron fraction of the disk at a given radius by balancing the time scale of deleptonization due to electron capture and subsequent neutrino emission against the time required to accrete to a given radius. Figure 7 shows the electron fraction for several analytic models computed by Surman and McLaughlin (2004). For comparison, we include the spherically averaged, density weighted electron fraction

$$\langle Ye \rangle_{\rm SADW}(r) = \frac{\int_{S^2} Ye\rho\sqrt{-g}d\Omega}{\int_{S^2} \rho\sqrt{-g}d\Omega} \qquad (15)$$

from this work, where g is the determinant of the metric and the integrals are over the 2-sphere. Recall that in the case of our full three-dimensional model, we used a black hole of mass $3M_\odot$ and a dimensionless spin parameter of $a = 0.8$. Note that these averages do not reflect the diversity of physical conditions present in a simulation. They capture the location of the disk as far as it has viscously spread, but they do not show properties of, e.g., disk turbulence, the jet, or the wind.

Except in the innermost parts of the disk, the electron fraction of the semi-analytic disk is well above the weak equilibrium value. This is because the neutrino emission is very sensitive to the temperature and is thus simply too slow to deleptonize the disk before it accretes.

In the semi-analytic models, the in-falling matter is neutral until densities and temperatures rise sufficiently, at which point electron fraction drops quickly. In contrast, we begin with a compact torus. Ideally, after sufficient time, this disk achieves a quasistationary state and "forgets" its initial conditions. However, this assumption is incompatible with the inflow-deleptonization

time scale assumption in the semi-analytic models. Material in the disk has *already* deleptonized before viscously spreading outward as it reaches a steady-state. Reconciling these two pictures requires performing a full physics simulation with the correct in-fall initial and boundary conditions.

McLaughlin and Surman (2005) and Surman *et al.* (2006) combined the electron fraction in the disks of Surman and McLaughlin (2004) with a wind model and calculated the composition of the wind ejecta, including the effects of absorption. They found that as material leaves the disk, Y_e rises and that subsequently very little low Y_e material is ejected in their models unless the accretion rate exceeds 1 $M_\odot s^{-1}$. Although these semi-analytic models are very different from our full-physics simulation, the key result is consistent.

5.2. *The Stabilizing Effect of the Initial Transient*

Although the core of the disk is low electron fraction, as described in sections 4.2 and 4.3, we find that almost none of the gravitationally unbound material is sufficiently low Y_e and high entropy to produce 3rd-peak r-process elements.

Figure 8 shows how this scenario changes if absorption is neglected, which we calculate by separately tracking changes in Y_e due to emission and absorption in our simulation. In the no-absorption scenario, the average electron fraction in the outflow erroneously drops from $\bar{Y}_e \approx 0.36$ to $\bar{Y}_e \approx 0.22$. This comparison implies that including absorption in these models is critical to correctly predicting nucleosynthetic yields in the outflow.

At late times, the neutrino optical depth is small, and yet we have found that treating absorption is critical to capturing the electron fraction in the outflow. Here we examine the initial transient that we neglect when considering the outflow. We find that this transient sets the electron fraction in the steady-state flow at late times, which may help keep the simulation consistent with a flow state set by in-fall as described in section 5.1.

One way of characterizing how much absorption matters is the neutrino optical depth τ. $\tau \ll 1$ implies a free-streaming limit, while $\tau \gg 1$ implies a diffusion limit (Castor 2004).[3] Once the disk reaches a quasi-stationary state, optical depths in the disk are low—of order 10^{-3}. However, at early times, during the transient phase, optical depths are of order unity.

The equilibrium torus used as an initial condition is close to the black hole and degeneracy pressures are high, causing disk material to rapidly deleptonize, as shown in the right panel of figure 9. As the disk disrupts, densities and temperatures rise near black hole, causing opacities, and thus optical depths, to become significant, as shown in the left panel of figure 9. The higher optical depths in this region prevent the electron fraction from dropping in this inner region. This inner material later sources the outflow.

In other words, neutrino absorption in this early phase *sets* the electron fraction of the outflow in the steady state. Note this does not mean that the steady-state remembers the initial conditions. Rather, it implies that, for the disk to reach the *correct* steady state, absorption

[3] Note that the relative volume density of leptons in the gas also matters.

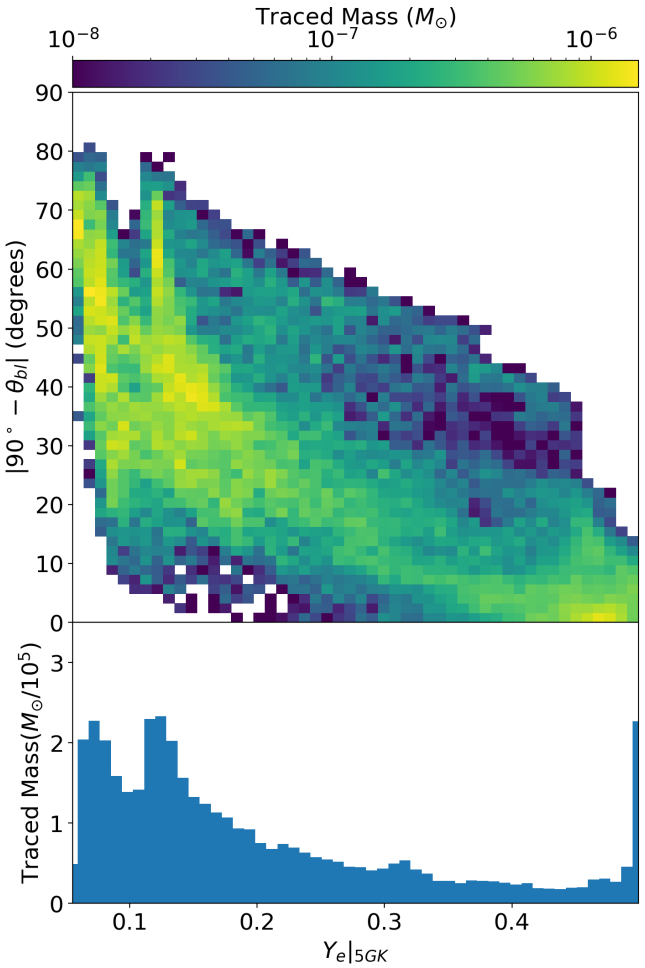

FIG. 8.— Electron fraction Y_e in the outflow, neglecting absorption. Top figure compares Y_e vs. angle and the bottom simply bins Y_e, weighted by tracer particle mass. In contrast to the full transport case, if absorption is neglected, the outflow contains low electron fraction material. The spike in $Y_e \approx 0.5$ is from viscous spreading at the back of the disk, which never drops to low electron fraction.

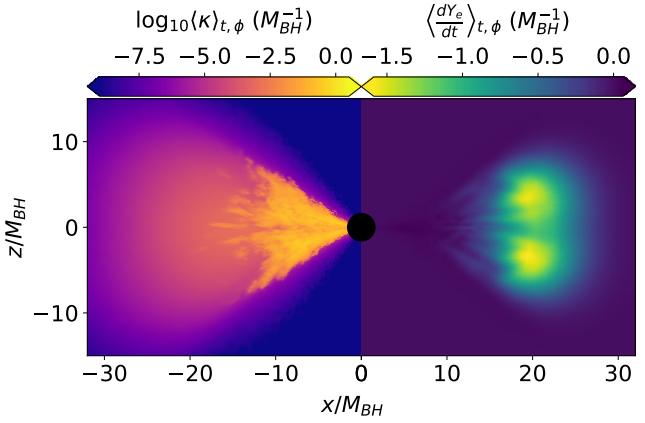

FIG. 9.— Neutrino opacity (left) and Lagrangian derivative of electron fraction in disk material (right). Both quantities are averaged over azimuthal angle ϕ and time in the early transient phase, from roughly 5 ms to 20 ms.

opacity must be accounted for.

5.3. *Effect of Stellar Envelope*

Section 4.2 assumes that all material with radius $r_e > 250GM_{BH}/c^2$ and positive Bernoulli parameter is gravitationally unbound. For an accretion disk in vacuum around a black hole, this is likely a reasonable assumption. However, in a collapsar scenario, the black hole-disk system is embedded in a collapsing star. For the wind to escape, it needs not only to escape the gravitational pull of the central black hole, but also of the star itself. Also unaccounted for is the ram pressure of in-falling material, as well as disruption of said fallback by the jet and convection and advection from the dynamics of the fallback material.

These effects, alone or together, may significantly change the amount of nucleosynthetic material which can escape the star. Understanding this requires better modeling of the disk-wind-envelope system and will be the subject of future work.

6. OUTLOOK AND IMPLICATIONS

We perform a three-dimensional general relativistic radiation magnetohydrodynamics disk simulation of a nucleosynthetically optimistic, high-accretion rate collapsar disk—the first to incorporate full neutrino transport.

We find that a steady state disk forms with electron fractions near the mid-plane as low as $Y_e \sim 0.15$. At higher latitudes, however, the electron fraction is significantly larger. This quasi-steady accretion flow drives a relatively neutron-poor outflow; there is almost no unbound material produced with electron fraction less than $Y_e \sim 0.3$.

We simulate r-process nucleosynthesis in this outflow via the PRISM reaction network (Mumpower *et al.* 2017; Zhu *et al.* 2018; Sprouse *et al.* 2019) and find almost no material with an atomic mass above $A \sim 130$ is produced. Our results thus imply that, even in the most nucleosynthetically optimistic case, wind-driven off of accretion disks in collapsars likely cannot act as a source for third-peak r-process elements. Indeed, since collapsars produce first- and second-peak r-process elements but not third-peak ones, including them as a significant source of light r-process elements at all may be in tension with the galactic chemical evolution and the solar abundance pattern (Côté *et al.* 2018).

We compare our model to the GRMHD model of Siegel *et al.* (2019) and the semi-analytic models developed in the literature (Popham *et al.* 1999; Di Matteo *et al.* 2002; Surman and McLaughlin 2004; McLaughlin and Surman 2005). We find the electron fraction in our disk is significantly higher than reported in Siegel *et al.* (2019), but lower than predicted in Surman and McLaughlin (2004); McLaughlin and Surman (2005). Moreover, we find that the electron fraction in our outflow is consistent with the semi-analytic picture.

A potential confounding factor in understanding the electron fraction in both the disk and the outflow is our use of a compact torus initial condition. This torus construction is a standard in the disk community. However, it is likely not appropriate for modeling a collapsar. First, the compact torus chosen provides a reservoir of material too close to the black hole, which means the gas does not have time to naturally deleptonize as it accretes. Second, the compact torus initial data ignores the presence of a star around and feeding the disk. As we discussed in section 5.3, the stellar envelope may have a significant effect on the mass in the outflow.

We argue that our discrepancy with Siegel *et al.* (2019) is related to how the initial conditions proceed to equilibrium when absorption is or is not included. Including absorption allows us to more closely match the flow state of a collapsar, where the disk is fed by fallback.

However, an obvious improvement is to use an initial condition that reflects the reality of a collapsing star. This strategy, adopted in the early work of MacFadyen and Woosley (1999). Such a strategy would also allow us to better understand exactly how much ejecta escapes the star. As discussed 5.3, this is difficult to address in a simulation that begins with an equilibrium torus. We will pursue such a program in future work.

We conclude by emphasizing three takeaway messages from our work. First, accurate treatments of neutrino transport and neutrino absorption are required to capture the evolution of Y_e. Second, initial conditions should be carefully considered for collapsar modeling. Finally, our model supports previous conclusions that even under optimistic assumptions, wind blown off of accretion disks in collapsars cannot act as a robust source of r-process material.

7. ACKNOWLEDGEMENTS

We thank Adam Burrows, Eliot Quataert, Charles Gammie, Jim Stone, Philipp Moesta, Luke Roberts, Benoit Cote, Sam Jones, Wes Even, Oleg Korobkin, Ryan Wollaeger, Sanjana Curtis, Greg Salvesen, and Daniel Siegel for many helpful discussions.

We acknowledge support from the U.S. Department of Energy Office of Science and the Office of Advanced Scientific Computing Research via the Scientific Discovery through Advanced Computing (SciDAC4) program and Grant DE-SC0018297

This work was supported by the US Department of Energy through the Los Alamos National Laboratory. Additional funding was provided by the Laboratory Directed Research and Development Program, the Center for Space and Earth Science (CSES), and the Center for Nonlinear Studies at Los Alamos National Laboratory under project numbers 20190021DR, 20180475DR (TS), and 20170508DR. This research used resources provided by the Los Alamos National Laboratory Institutional Computing Program. Los Alamos National Laboratory is operated by Triad National Security, LLC, for the National Nuclear Security Administration of U.S. Department of Energy under Contract No. 89233218CNA000001.

This article is cleared for unlimited release, LA-UR-19-30392.

We are grateful to the countless developers contributing to open source projects on which we relied in this work, including Python (Rossum 1995), the GNU compiler (Stallman and Developer Community 2009), numpy and scipy (van der Walt *et al.* 2011; Jones *et al.* 01), Matplotlib (Hunter 2007), the GNU scientific library (Galassi and Gough 2009), and HDF5 (The HDF Group 2019).

REFERENCES

S. E. Woosley, ApJ **405**, 273 (1993).
A. I. MacFadyen and S. E. Woosley, The Astrophysical Journal **524**, 262 (1999).
S. E. Woosley and J. S. Bloom, ARA&A **44**, 507 (2006), astro-ph/0609142.
G. Ghirlanda, L. Nava, G. Ghisellini, A. Celotti, and C. Firmani, A&A **496**, 585 (2009), arXiv:0902.0983 [astro-ph.HE].
J. Hjorth and J. S. Bloom, in *Gamma-Ray Bursts*, edited by C. Kouveliotou, R. Wijers, and S. Woosley (Cambridge University Press, Cambridge, Cambridge, 2012) Chap. 9, pp. 169–189.
A. I. MacFadyen, S. E. Woosley, and A. Heger, ApJ **550**, 410 (2001), astro-ph/9910034.
D. Proga, A. I. MacFadyen, P. J. Armitage, and M. C. Begelman, The Astrophysical Journal **599**, L5 (2003), arXiv:astro-ph/0310002 [astro-ph].
A. Heger, C. L. Fryer, S. E. Woosley, N. Langer, and D. H. Hartmann, ApJ **591**, 288 (2003), arXiv:astro-ph/0212469 [astro-ph].
Y. Mizuno, S. Yamada, S. Koide, and K. Shibata, ApJ **606**, 395 (2004), astro-ph/0404152.
S.-i. Fujimoto, K. Kotake, S. Yamada, M.-a. Hashimoto, and K. Sato, ApJ **644**, 1040 (2006), astro-ph/0602457.
S. Nagataki, R. Takahashi, A. Mizuta, and T. Takiwaki, ApJ **659**, 512 (2007), astro-ph/0608233.
G. Rockefeller, C. L. Fryer, and H. Li, arXiv e-prints , astro-ph/0608028 (2006), arXiv:astro-ph/0608028 [astro-ph].
D. A. Uzdensky and A. I. MacFadyen, ApJ **669**, 546 (2007), astro-ph/0609047.
B. J. Morsony, D. Lazzati, and M. C. Begelman, ApJ **665**, 569 (2007), astro-ph/0609254.
N. Bucciantini, E. Quataert, J. Arons, B. D. Metzger, and T. A. Thompson, MNRAS **383**, L25 (2008), arXiv:0707.2100.
D. Lazzati, R. Perna, and M. C. Begelman, MNRAS **388**, L15 (2008), arXiv:0805.0138.
P. Kumar, R. Narayan, and J. L. Johnson, MNRAS **388**, 1729 (2008), arXiv:0807.0441.
H. Nagakura, H. Ito, K. Kiuchi, and S. Yamada, ApJ **731**, 80 (2011), arXiv:1009.2326 [astro-ph.HE].
P. A. Taylor, J. C. Miller, and P. Podsiadlowski, MNRAS **410**, 2385 (2011), arXiv:1006.4624 [astro-ph.HE].
C. D. Ott, C. Reisswig, E. Schnetter, E. O'Connor, U. Sperhake, F. Löffler, P. Diener, E. Abdikamalov, I. Hawke, and A. Burrows, Phys. Rev. Lett. **106**, 161103 (2011).
C. C. Lindner, M. Milosavljević, R. Shen, and P. Kumar, ApJ **750**, 163 (2012), arXiv:1108.1415 [astro-ph.HE].
D. López-Cámara, B. J. Morsony, M. C. Begelman, and D. Lazzati, ApJ **767**, 19 (2013), arXiv:1212.0539 [astro-ph.HE].
A. Batta and W. H. Lee, MNRAS **437**, 2412 (2014), arXiv:1307.2339 [astro-ph.HE].
T. A. Thompson, P. Chang, and E. Quataert, ApJ **611**, 380 (2004), astro-ph/0401555.
B. D. Metzger, T. A. Thompson, and E. Quataert, ApJ **676**, 1130 (2008), arXiv:0708.3395.
C. Winteler, R. Käppeli, A. Perego, A. Arcones, N. Vasset, N. Nishimura, M. Liebendörfer, and F.-K. Thielemann, ApJ **750**, L22 (2012), arXiv:1203.0616 [astro-ph.SR].
P. Mösta, S. Richers, C. D. Ott, R. Haas, A. L. Piro, K. Boydstun, E. Abdikamalov, C. Reisswig, and E. Schnetter, ApJ **785**, L29 (2014), arXiv:1403.1230 [astro-ph.HE].
P. Mösta, L. F. Roberts, G. Halevi, C. D. Ott, J. Lippuner, R. Haas, and E. Schnetter, ApJ **864**, 171 (2018), arXiv:1712.09370 [astro-ph.HE].
G. Halevi and P. Mösta, MNRAS **477**, 2366 (2018), arXiv:1801.08943 [astro-ph.HE].
S. I. Blinnikov *et al.*, Soviet Astronomy Letters **10**, 177 (1984), arXiv:1808.05287 [astro-ph.HE].
J. M. Lattimer and D. N. Schramm, ApJ **210**, 549 (1976).
J. M. Lattimer, F. Mackie, D. G. Ravenhall, and D. N. Schramm, ApJ **213**, 225 (1977).
R. Popham *et al.*, The Astrophysical Journal **518**, 356 (1999).
T. Di Matteo, R. Perna, and R. Narayan, ApJ **579**, 706 (2002), astro-ph/0207319.
R. Surman and G. C. McLaughlin, The Astrophysical Journal **603**, 611 (2004).
G. C. McLaughlin and R. Surman, Nuclear Physics A **758**, 189 (2005), arXiv:astro-ph/0407555 [astro-ph].
R. Surman, G. C. McLaughlin, and W. R. Hix, The Astrophysical Journal **643**, 1057 (2006).
G. Rockefeller, C. L. Fryer, P. Young, M. Bennett, S. Diehl, F. Herwig, R. Hirschi, A. Hungerford, M. Pignatari, G. Magkotsios, and F. X. Timmes, arXiv e-prints , arXiv:0811.4650 (2008), arXiv:0811.4650 [astro-ph].
S.-i. Fujimoto, M.-a. Hashimoto, K. Kotake, and S. Yamada, ApJ **656**, 382 (2007), astro-ph/0602460.
M. Ono, M. Hashimoto, S. Fujimoto, K. Kotake, and S. Yamada, Progress of Theoretical Physics **128**, 741 (2012), arXiv:1203.6488 [astro-ph.SR].
K. Nakamura, T. Kajino, G. J. Mathews, S. Sato, and S. Harikae, A&A **582**, A34 (2015).
N. Soker and A. Gilkis, ApJ **851**, 95 (2017), arXiv:1708.08356 [astro-ph.HE].
T. Hayakawa and K. Maeda, ApJ **854**, 43 (2018), arXiv:1801.09681 [astro-ph.HE].
T. G. Cowling, MNRAS **94**, 39 (1933).
T. G. Cowling, The Quarterly Journal of Mechanics and Applied Mathematics **10**, 129 (1957).
D. M. Siegel, J. Barnes, and B. D. Metzger, Nature **569**, 241 (2019), arXiv:1810.00098 [astro-ph.HE].
M. Liebendörfer, ApJ **633**, 1042 (2005), arXiv:astro-ph/0504072 [astro-ph].
E. O'Connor and C. D. Ott, Classical and Quantum Gravity **27**, 114103 (2010), arXiv:0912.2393 [astro-ph.HE].
J. M. Miller, B. R. Ryan, J. C. Dolence, A. Burrows, C. J. Fontes, C. L. Fryer, O. Korobkin, J. Lippuner, M. R. Mumpower, and R. T. Wollaeger, Phys. Rev. D **100**, 023008 (2019a), arXiv:1905.07477 [astro-ph.HE].
A. W. Steiner, M. Hempel, and T. Fischer, ApJ **774**, 17 (2013), arXiv:1207.2184 [astro-ph.SR].
E. O'Connor and C. D. Ott, Classical and Quantum Gravity **27**, 114103 (2010).
M. A. Skinner, J. C. Dolence, A. Burrows, D. Radice, and D. Vartanyan, ApJS **241**, 7 (2019), arXiv:1806.07390 [astro-ph.IM].
A. Burrows, S. Reddy, and T. A. Thompson, Nuclear Physics A **777**, 356 (2006), astro-ph/0404432.
J. M. Miller, B. R. Ryan, and J. C. Dolence, The Astrophysical Journal Supplement Series **241**, 30 (2019b).
R. P. Kerr, Phys. Rev. Lett. **11**, 237 (1963).
L. G. Fishbone and V. Moncrief, ApJ **207**, 962 (1976).
S. A. Balbus and J. F. Hawley, ApJ **376**, 214 (1991).
N. I. Shakura and R. A. Sunyaev, Astronomy and Astrophysics **500**, 33 (1973).
B. R. Ryan, J. C. Dolence, and C. F. Gammie, The Astrophysical Journal **807**, 31 (2015).
C. F. Gammie, J. C. McKinney, and G. Tóth, The Astrophysical Journal **589**, 444 (2003).
J. C. Dolence, C. F. Gammie, M. Mościbrodzka, and P. K. Leung, The Astrophysical Journal Supplement Series **184**, 387 (2009).
L. Bovard and L. Rezzolla, Classical and Quantum Gravity **34**, 215005 (2017), arXiv:1705.07882 [gr-qc].
T. Sano, S. ichiro Inutsuka, N. J. Turner, and J. M. Stone, The Astrophysical Journal **605**, 321 (2004).
J. F. Hawley, S. A. Richers, X. Guan, and J. H. Krolik, ApJ **772**, 102 (2013), arXiv:1306.0243 [astro-ph.IM].
M. Arnould, S. Goriely, and K. Takahashi, Physics Reports **450**, 97 (2007), arXiv:0705.4512.
M. R. Mumpower, T. Kawano, J. L. Ullmann, M. Krtička, and T. M. Sprouse, Physical Review C **96** (2017), 10.1103/PhysRevC.96.024612.
B. Côté *et al.*, ApJ **855**, 99 (2018), arXiv:1710.05875.
Y. Zhu, R. T. Wollaeger, N. Vassh, R. Surman, T. M. Sprouse, M. R. Mumpower, P. Möller, G. C. McLaughlin, O. Korobkin, T. Kawano, P. J. Jaffke, E. M. Holmbeck, C. L. Fryer, W. P. Even, A. J. Couture, and J. Barnes, The Astrophysical Journal **863**, L23 (2018).
T. M. Sprouse, R. N. Perez, R. Surman, M. R. Mumpower, G. C. McLaughlin, and N. Schunck, submitted to Physical Review (2019), arXiv: 1901.10337.

R. H. Cyburt, A. M. Amthor, R. Ferguson, Z. Meisel, K. Smith, S. Warren, A. Heger, R. D. Hoffman, T. Rauscher, A. Sakharuk, H. Schatz, F. K. Thielemann, and M. Wiescher, ApJS **189**, 240 (2010), REACLIB is available at `https://groups.nscl.msu.edu/jina/reaclib/db/`.

T. Kawano, R. Capote, S. Hilaire, and P. Chau Huu-Tai, Physical Review C **94**, 014612 (2016).

P. Möller, W. D. Myers, H. Sagawa, and S. Yoshida, Physical Review Letters **108**, 052501 (2012).

M. R. Mumpower, T. Kawano, and P. Möller, Phys. Rev. C **94**, 064317 (2016).

M. R. Mumpower, T. Kawano, T. M. Sprouse, N. Vassh, E. M. Holmbeck, R. Surman, and P. Möller, ApJ **869**, 14 (2018), arXiv:1802.04398 [nucl-th].

P. Möller, M. Mumpower, T. Kawano, and W. Myers, Atomic Data and Nuclear Data Tables **125**, 1 (2019).

G. Audi, F. G. Kondev, M. Wang, W. J. Huang, and S. Naimi, Chinese Physics C **41**, 030001 (2017).

M. Wang, G. Audi, F. G. Kondev, W. J. Huang, S. Naimi, and X. Xu, Chinese Phys. C **41**, 030003 (2017).

J. Castor, *Radiation Hydrodynamics*, Radiation Hydrodynamics (Cambridge University Press, 2004).

G. Rossum, *Python Reference Manual*, Tech. Rep. (Amsterdam, The Netherlands, The Netherlands, 1995).

R. Stallman and Developer Community, *Using the Gnu Compiler Collection: A Gnu Manual for Gcc Version 4.3.3* (SoHo Books, 2009).

S. van der Walt, S. C. Colbert, and G. Varoquaux, Computing in Science Engineering **13**, 22 (2011).

E. Jones *et al.*, "SciPy: Open source scientific tools for Python," (2001–), `http://www.scipy.org/`.

J. D. Hunter, Computing In Science & Engineering **9**, 90 (2007).

M. Galassi and B. Gough, *GNU Scientific Library: Reference Manual*, GNU manual (Network Theory, 2009).

The HDF Group, "Hierarchical Data Format, version 5," (1997-2019), `http://www.hdfgroup.org/HDF5/`